Dynamic Ionic Clusters with Flowing Electron Bubbles from Warm to Hot Dense Iron along the Hugoniot Curve

Jiayu Dai,[1] Dongdong Kang,[1] Zengxiu Zhao,[1] Yanqun Wu,[2] and Jianmin Yuan[1,3,*]

[1]*Department of Physics, College of Science, National University of Defense Technology,
Changsha 410073, People's Republic of China*
[2]*College of Optoelectric Science and Engineering, National University of Defense Technology,
Changsha 410073, People's Republic of China*
[3]*State Key Laboratory of High Performance Computing, National University of Defense Technology,
Changsha 410073, People's Republic of China*

Complex structures of warm and hot dense matter are essential to understanding the behavior of materials in high energy density processes and provide new features of matter constitutions. Here, around a new unified first-principles determined Hugoniot curve of iron from the normal condensed condition up to 1 Gbar, the novel structures characterized by the ionic clusters with *electron bubbles* are found using quantum Langevin molecular dynamics. Subsistence of complex clusters can persist in the time scale of 50 fs dynamically with quantum flowing bubbles, which are produced by the interplay of Fermi electron degeneracy, the ionic coupling, and the dynamical nature. With the inclusion of those complicated features in quantum Langevin molecular dynamics, the present equation of states could serve as a first-principles based database in a wide range of temperatures and densities.

The thermodynamic and structural properties of matter at extreme conditions, the so-called warm dense matter (WDM) and hot dense matter (HDM) in the field of high energy density physics (HEDP) [1], are both experimental and theoretical challenges and crucial to the comprehension of giant planets, stars, inertial confinement fusion target capsules, as well as materials science [1–8]. New physics discovered by high-power laser facilities such as the National Ignition Facility and nuclear fusion [9–14] requires understanding beyond traditional condensed matter, atomic, and plasma physics [1,6]. Recent laser-driven dynamical experiments and related theories have shown the existence of ordered electron-ion structures [14–21] and electronic bonds [12,22] in HEDP with x-ray methods, suggesting the necessity of taking into account the dynamics of local chemical environments. Meanwhile, studies of static high-pressure theories and experiments have led to the finding of *electron blobs* formed by valence electrons and new-type electronic bonds assisted by inner-shell electrons [23–25]. However, for lack of effective methods, few theoretical studies are being carried out on the structures of complex materials in the field of HEDP. In HDM, the densities and temperatures are comparable to or even much higher than the states of static compressions and WDM [1,9]. Higher density could induce new features that cannot be observed in the normal WDM, while higher temperature induces dynamical changes of the ionic configurations accompanied by dynamical electronic distributions. The properties of matter, including the equation of states (EOS), electronic and ionic transport, and optical properties, depend on the

details of the electron-ion structures being explored under these extreme conditions.

In order to shed light on the hidden features and controversial intrinsic dynamics from WDM to HDM, the electron-ion structures are calculated along the newly determined principal Hugoniot curve of Fe using quantum Langevin molecular dynamics (QLMD) [26,27]. For Fe, as one of the most abundant elements in the Universe and a typical complicated transition metal, it has been a long-standing challenge [3–5,14,28–32] to obtain its physical properties, because of the strong ionic coupling and high electronic degeneracy over a wide range of temperatures and densities. To date, previous experiments and statistical theories have generated abundant results with a large divergence and uncertainty in the EOS [28–32]. First-principles studies on the EOS and electronic properties of crystalline or liquid Fe at high pressure and zero or relatively low temperature have been widely reported [3–5,33,34], and a few fixed density-temperature (*D-T*) points on the Hugoniot curve picked up from SESAME tables were calculated by quantum molecular dynamics (QMD) [27,28]. However, the Hugoniot data beyond WDM from first principles are never covered.

QLMD or QMD, based on the finite-temperature density functional theory (DFT) [35], can naturally include electron-ion interactions and the effects of degeneracy and coupling contributing to the pressure and energy, and has been successfully applied to derive the EOS and dynamical properties of dense matter including Fe [2,33,34,36–40]. Advantageously, QLMD, adopted in the QUANTUM ESPRESSO package [41], can be extended to the

HEDP field within the *ab initio* framework by introducing electron-ion collisions induced friction [27], validated by comparison with other results from experiments and path integral Monte Carlo (PIMC) methods on light elements [27,39,40]. It is thus possible to accurately explore the details of the electron-ion structures in WDM and HDM. In the present work, 54 atoms are included in the supercell with $3 \times 3 \times 3$ k points below 10 eV and only the Γ point at higher temperatures for the representation of the Brillouin zone. A pseudopotential with 16 valence electrons within the generalized-gradient approximation (GGA) [42,43] is used. During the molecular dynamics processes, the time steps are from 1 to 0.25 fs with increasing temperatures, and a 2 ps time length is used to achieve the thermal stability state. After the thermalization, a time length of more than 2 ps is used to acquire the thermal properties. About 300 D-T points are calculated in order to get the EOS data [43].

The EOS of the temperatures from 0.1 to 100 eV and pressures up to 1 Gbar (1 Gbar = 100 TPa) on both sides of the Hugoniot curve are obtained. One of the most spectacular physical results here is the electronic structures in HDM, which are rarely known today. To dig out these features, the electronic distributions at the highest pressure (1.122 Gbar) with a D-T point of (48.23 g/cm^3, 100 eV) are displayed. The formation of *blobs* of valence electrons between the ions of cold Fe with pressure of 158 Mbar [33,43] is shown in Fig. 1(a), which has been identified in

FIG. 1 (color). The electronic charge density (electron/Å^3) distributions of iron. (a) and (b): Three- and two-dimensional contour plot in the (010) direction for the charge density of iron in fcc phase at (0 eV, 48.23 g/cm^3) below 65% of its maximum value, yellow balls represent the Fe ions; the pink or gray color represents the electron blobs; (c) and (d): the same contour plot of iron at (100 eV, 48.23 g/cm^3).

cold compressed aluminum [24] and sodium [25]. Furthermore, the inner s, p electrons will assist the bonding on Fe-Fe, as shown in the band structures in recent high-density results [33]. This can also be shown in the two-dimensional density distribution in Fig. 1(b), where the green *blobs* are distributed between the Fe ions. How does this feature change when the dynamical effects are introduced? As shown in Fig. 1(c), the valence electron "blobs" tend to assemble together and form bigger *bubbles* in the interspaces of the Fe ions. These freelike electrons are distributed inhomogenously and behave as *quantum electron liquids* flowing with ionic movement. It can be observed in the two-dimensional picture in Fig. 1(d), where some free electrons (green color) are distributed in the interspaces of the ions. Interestingly, there are clearcut density overlaps (see Fig. S10 in Supplemental Material Ref. [43]) among some ions here induced by the inner orbital electrons, indicating the existence of many-body bonding formed by inner-shell electrons. To verify the existence of *bubbles*, more than ten snapshots of the ionic configurations are chosen randomly (see Fig. S11 in Supplemental Material Ref. [43]), where the *bubbles* are always there but with different shapes from the high-accuracy self-consistent calculations (dense k points and small convergence tolerances). Here, the *bubbles* are formed by the interplay of the Fermi electron degeneracy, the ionic coupling, and the temperature-induced dynamics, which are different from the electron bubbles in helium at low temperatures [44] (formed by excess electrons) and in laser induced plasma [45] (formed by an electric field gradient).

The electronic distributions also show the complexity of the ionic structures, whose details and dynamics are still elusive. Most importantly, the electronic structures are sensitively dependent on the dynamics of the ions and their collective behaviors. In order to understand the physics of the dynamical structures, we select five D-T points as shown in Fig. 2 along the new principal Hugoniot curve. Their radial distribution function (RDF) shown in Fig. 2(a) gives evidence of a transition in the ionic structures from long-range to short-range order statistically. It is worth noting that even at $T = 100$ eV, there is one peak in the RDF, indicating the existence of hidden ordered structures. Considering the short-range ordered structures at high temperatures, we borrow the language of liquid structures such as water and clusters to reveal the structures in HEDP, i.e., the orientation order parameter $Q = 1 - \frac{3}{8}\sum_{i=1}^{3}\sum_{j=i+1}^{4}(\cos\theta_{ij} + \frac{1}{3})^2$, where θ_{ij} is the angle formed by the lines of an ion and its nearest neighbors i and j (≤ 4). The value of Q, varying from 0 (in an ideal gas) to 1 (in a perfect tetrahedral network), can be used as a measurement of tetrahedrality for the local coordination structure [46,47]. As shown in Fig. 2(b), the peak of the distribution of the parameter Q shifts from 0.45 to 0.35 with increasing temperature, indicating that the ionic structures
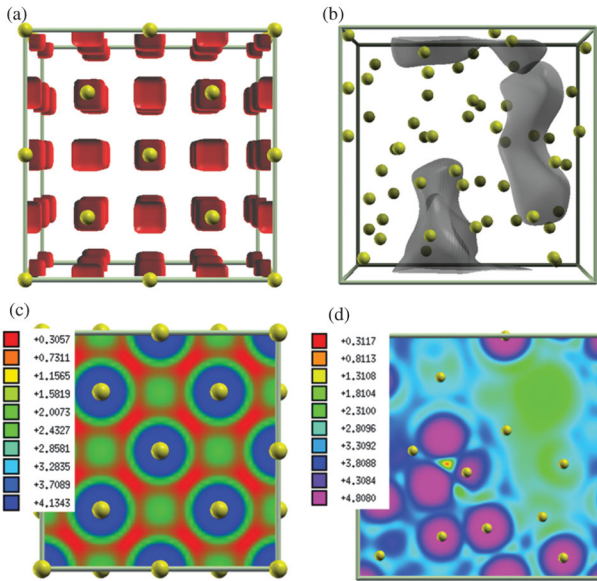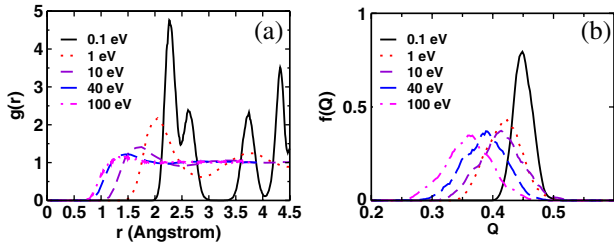
FIG. 2 (color online). (a) RDF and (b) the distribution of orientation order parameters Q for the selected five temperature-density points along Hugoniot curve. The corresponding temperatures and densities are respectively 0.1, 1, 10, 40, and 100 eV, and 10.1, 13.23, 18.75, 28.875, and 33.385 g/cm^3.
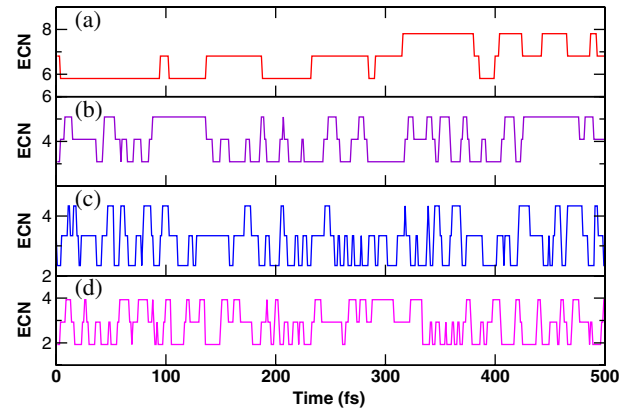

FIG. 3 (color online). Trajectories of ECNs for a specific atom during the of 0.5 ps time length simulations at different states of (a) 0.1 eV, (b) 1 eV, (c) 10 eV, and (d) 100 eV, respectively.

with the ideal tetrahedral network indeed collapse but that there are still some similar topological structures.

Some ordered structures survive even at 100 eV from the hints of Figs. 1 and 2. However, there is not a clear minimum after the first peak in the RDF in Fig. 2(a) except for 0.1 eV. Therefore, a dissociation criterion based solely on a hard cutoff of Fe-Fe bond lengths would be optional. The probability distribution of the coordination numbers (CNs) can be appropriate for analyzing the local geometry, which has been successfully used for estimating the dissociation of water molecules at high temperatures [48]. Due to the short-range ordered structures in HDM [49], here we adopted the idea of effective CNs (ECNs) [43,50]. For low-symmetry structures where a specific atom is surrounded by atoms at different distances, the ECN concept can be independent of the choice of the bond cutoff, and therefore provides a more accurate method to determine possible structural trends in disordered structures.

For the above five D-T points, the ECNs decrease from 10.99 to 2.93 Å, whose corresponding average bond lengths are from 2.33 to 1.15 Å. With increasing temperatures and densities, the ECNs decrease gradually, but remain larger than unity even up to 100 eV. This fact indicates the existence of clusterlike or networklike structures, which is consistent with the hints in Fig. 1. Some of the ions catch only one nearest neighbor (ECN = 1) when the temperature is high enough, indicating the formation of two-ion chains. The distributed percentages of these *chains* are 13, 26, and 36%, respectively, for temperatures of 10, 40 and 100 eV. Furthermore, the differences between the dynamical average bond lengths and ionic radii (from 2.10 to 1.41 Å) show that the interatomic distances cannot be simply described by the hard sphere model corresponding to the density.

The understanding of the dynamics of these bond-network breaking and forming patterns is also necessary since an instantaneous topological structure cannot affect the observed properties obviously. To investigate the structural dynamics, we first trace the topological networks around one specific atom, as shown in Fig. 3. With increasing temperature, the movements of ions in the liquid states

introduce physical processes such as dissociations [48], resulting in the changes of structures. However, even though the structures exhibit dynamical changes, a considerable fraction of ions in warm and hot dense Fe with compact clusters can persist for times as long as a few tens of femtoseconds even at $T = 100$ eV. Because most ECN_i values are centered around the ECN within the value of 2 (Fig. S3 in Supplemental Material [43]), only three patterns of topological structures are statistically averaged: using ECN as the reference, for the ith atom, we assume $ECN_i = ECN - 1$ when $ECN_i \leq ECN - 1$, $ECN_i = ECN + 1$ when $ECN_i \geq ECN + 1$, and $ECN_i = ECN$ when $ECN - 1 < ECN_i < ECN + 1$. Summing up the persistent time length for each structure, we find that more than 15% of the structures forms and breaks up on a time scale of longer than 20 fs at 100 eV (Fig. S4 in Supplemental Material [43]). With the moving clusterlike ions, the *electron bubbles* will be transported between the interspaces of the different clusters as flowing fluids. These bubbles may crash at one time, but will appear at the next time with different configurations in different interspaces. The clusters will persist long enough at the time scale and high enough at the percentage to affect the electronic structures and related properties such as energies, optical properties, and electronic conductivities [49]. The *bubbles* and the ionic clusters will persist at the same time scale, since they are correlated and generated simultaneously. This understanding violates the traditional assumption that the states at so high a temperature can be modeled at the single atomic scale. On the contrary, the collective and quantum essentials must be treated appropriately. Furthermore, the dynamical behaviors of the topological structures introduce a challenge for statistical models such as the hypernetted-chain (HNC) theory [17,18] to include more topological networks in its constructed potentials. From another point of view, the dominant two- or three-ion chain structures at the temperature of 100 eV would
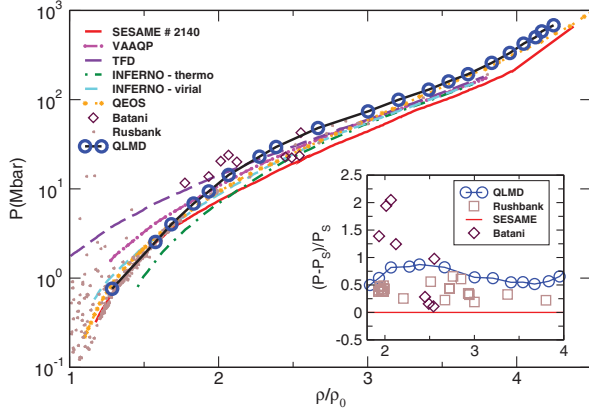
FIG. 4 (color). Principal Hugoniot of Fe, comparing the results from QLMD with other models and experiments. The corresponding temperatures are 0.1, 0.5, 1, 2, 3, 5, 8, 10, 15, 20, 25, 30, 35, 40, 50, 60, 70, 80, 90, and 100 eV. Inset shows the deviations of QLMD, Rushbank, and Batani's data from SESAME tables (P_S).

induce closer pressures between the statistical methods and QLMD [27,28] methods due to the simple structures.

Let us go back to the principal Hugoniot curve in Fig. 4, which is determined by interpolating a few density points at a fixed temperature according to the Hugoniot-Rankine relation [36,51]: $(U - U_0) = \frac{1}{2}(P + P_0)(V_0 - V)$, where U, P, and V are the internal energy, the total pressure, and the volume of the system, respectively; U_0, P_0, V_0 are the respective parameters of the initial reference state (7.86 g/cm^3 and 20 K). Twenty Hugoniot D-T points are determined up to the pressure of 1 Gbar, as shown in Fig. 4. It is of note that the spin polarization is important at $T = 0.1$ eV.

The previous experimental and theoretical data are scattered [5,30], especially in the WDM near the pressure of a few Mbar. In this regime, our first-principles results are along the lower limit envelope of the distributions of the experimental data, similar to the SESAME tables. Compared with the results of statistical methods such as the Thomas-Fermi-Dirac (TFD) [28], variational-average-atom-in-quantum-plasmas (VAAQP), INFERNO [31], and quotidian equation of state (QEOS) [52] models, the Hugoniot curve derived from QLMD is much closer to the data from Rusbank and Batani's experiment [29,30], especially with pressures above 10 Mbar. In particular, the deviations of the QLMD results from Rushbank and Batani's data and SESAME tables can reach to 60, 100 and 90% around the compressed ratio of 2.0, but the QLMD results are already located in the middle of the experiments, as shown in Fig. 4. In experiments, external factors such as preheating can affect the final results significantly [30], inducing unexpected higher pressures. The SESAME tables are far from both the experimental data and our data at relatively high temperatures, also shown by previous studies [30,53]. Because of the inclusion of

many-body interactions, collective quantum electronic distributions, and their dynamics at high densities and temperatures, the internal energies from QLMD should be lower than those of statistical models according to the variational principle. Lower internal energies at a definite pressure would result in lower densities. Therefore, the Hugoniot curve derived from QLMD would be higher than those of the others. This is the reason for the results of harder compression from first principles [2,38].

Finally, we construct the formula of all calculated EOS, i.e., in the range of $0.5 \leq T \leq 100$ eV, $9 \leq \rho \leq 45$ g/cm^3. This study is important for the applications of our data to the experimental comparisons and hydrodynamics. The optimal fit formula in a least-squares sense is as follows according to the virial expansions using a typical EOS relation:

$$P(T, \rho) = \sum_{m=0}^{M}\left[\sum_{n=0}^{N} \alpha_{mn}(\log_{10}T)^n\right]\rho^m, \quad (M=2, N=12),$$

(1)

where the units of P, T, and ρ are kbar, K, and g/cm^3, respectively. The values of the coefficients α_{mn} and the validation are shown in the Supplemental Material [43]. This is also important for the off Hugoniot curve and isentropic compressions.

In conclusion, the free electron *blobs* in cold dense matter move and assemble together, forming bigger *bubbles* between clusterlike ions at high temperatures, and exhibiting as quantum fluids. The dynamical ionic structures are analyzed according to the topological structures based on the ECN concept, giving a new realization of the stable existence of compact clusters contributed by the inner-shell electrons forming bonds even at $T = 100$ eV. The ionic structures with bound electrons can be compared to the soft *skeleton* in the system, which are expected to be responsible for the shearing strength, viscosity, and response to the shock waves, while the free electrons can be compared to *protoplasm* flowing among the skeletons contributing to the kinetic pressure of the electrons, and conductivities, since different structures will give rise to different response properties [54]. In addition, these unique features would raise a challenge to understand the dynamical formation of ordered structures from nonequilibrium to equilibrium. Last, the new Hugoniot data from QLMD simulations provide the parameter-free EOS of Fe, which can be regarded as the converged limit of the error-free experimental data.

*jmyuan@nudt.edu.cn

[1] F. R. Graziani *et al.*, High Energy Density Phys. **8**, 105 (2012).

[2] S. X. Hu, B. Militzer, V. N. Goncharov, and S. Skupsky, Phys. Rev. Lett. **104**, 235003 (2010).

[3] D. Alfè, M. J. Gillan, and G. D. Price, Nature (London) **401**, 462 (1999).

[4] A. B. Belonoshko, N. V. Skorodumova, A. Rosengren, and B. Johansson, Science **319**, 797 (2008).

[5] S. Tateno, K. Hirose, Y. Ohishi, and Y. Tatsumi, Science **330**, 359 (2010).

[6] J. Dai, Y. Hou, and J. Yuan, Astrophys. J. **721**, 1158 (2010).

[7] S. Ichimaru, Rev. Mod. Phys. **54**, 1017 (1982).

[8] D. C. Swift, J. H. Eggert, D. G. Hicks, S. Hamel, K. Caspersen, E. Schwegler, G. W. Collins, N. Nettelmann, and G. J. Ackland, Astrophys. J. **744**, 59 (2012).

[9] E. I. Moses, R. N. Boyd, B. A. Remington, C. J. Keane, and R. Al-Ayat, Phys. Plasmas **16**, 041 006 (2009).

[10] J. H. Eggert , D. G. Hicks, P. M. Celliers, D. K. Bradley, R. S. McWilliams, R. Jeanloz, J. E. Miller, T. R. Boehly, and G. W. Collins, Nature Phys. **6**, 40 (2010).

[11] R. Jeanloz, P. M. Celliers, G. W. Collins, J. H. Eggert, K. K. M. Lee, R. S. McWilliams, S. Brygoo, and P. Loubeyre, Proc. Natl. Acad. Sci. U.S.A. **104**, 9172 (2007).

[12] R. Ernstorfer, M. Harb, C. T. Hebeisen, G. Sciaini, T. Dartigalongue, and R. J. D. Miller, Science **323**, 1033 (2009).

[13] S. H. Glenzer *et al.*, Nature Phys. **3**, 716 (2007).

[14] R. F. Trunin, Phys. Usp. **37**, 1123 (1994).

[15] A. Mančić *et al.*, Phys. Rev. Lett. **104**, 035002 (2010).

[16] F. Dorchies *et al.*, Phys. Rev. Lett. **107**, 245006 (2011).

[17] K. Wünsch, J. Vorberger, and D. O. Gericke, Phys. Rev. E **79**, 010201(R) (2009).

[18] M. W. C. Dharma-wardana and M. S. Murillo, Phys. Rev. E **77**, 026401 (2008).

[19] E. G. Saiz *et al.*, Nature Phys. **4**, 940 (2008).

[20] S. H. Glenzer and R. Redmer, Rev. Mod. Phys. **81**, 1625 (2009).

[21] S. Mazevet and G. Zérah, Phys. Rev. Lett. **101**, 155001 (2008).

[22] J. T. Okada *et al.*, Phys. Rev. Lett. **108**, 067402 (2012).

[23] B. Rousseau and N. W. Ashcroft, Phys. Rev. Lett. **101**, 046407 (2008).

[24] C. J. Pickard and R. J. Needs, Nature Mater. **9**, 624 (2010).

[25] Y. Ma, M. Eremets, A. R. Oganov, Y. Xie, I. Trojan, S. Medvedev, A. O. Lyakhov, M. Valle, and V. Prakapenka, Nature (London) **458**, 182 (2009).

[26] J. Dai and J. Yuan, Europhys. Lett. **88**, 20 001 (2009).

[27] J. Dai, Y. Hou, and J. Yuan, Phys. Rev. Lett. **104**, 245001 (2010).

[28] F. Lambert, J. Clérouin, and G. Zérah, Phys. Rev. E **73**, 016403 (2006).

[29] A. V. Bushman *et al.*, Ihed Shock Wave Database, http://www.ihed.ras.ru/rusbank/.

[30] D. Batani *et al.*, Phys. Rev. Lett. **88**, 235502 (2002).

[31] R. Piron and T. Blenski, Phys. Rev. E **83**, 026403 (2011).

[32] S. P. Lyon and J. D. Johnson, Los Alamos National Laboratory Report No. LA-UR-92-3407, 1992.

[33] L. Stixrude, Phys. Rev. Lett. **108**, 055505 (2012).

[34] C. J. Pickard and R. J. Needs, J. Phys. Condens. Matter **21**, 452 205 (2009).

[35] N. D. Mermin, Phys. Rev. **137**, A1441 (1965).

[36] M. P. Surh, T. W. Barbee, and L. H. Yang, Phys. Rev. Lett. **86**, 5958 (2001).

[37] L. Collins, I. Kwon, J. Kress, N. Troullier, and D. Lynch, Phys. Rev. E **52**, 6202 (1995); M. P. Desjarlais, J. D. Kress, and L. A. Collins, *ibid.* **66**, 025401(R) (2002); S. Mazevet, M. P. Desjarlais, L. A. Collins, J. D. Kress, and N. H. Magee, *ibid.* **71**, 016409 (2005).

[38] M. D. Knudson and M. P. Desjarlais, Phys. Rev. Lett. **103**, 225501 (2009).

[39] B. Militzer and D. M. Ceperley, Phys. Rev. E **63**, 066404 (2001); B. Militzer, Phys. Rev. B **79**, 155105 (2009).

[40] K. P. Driver and B. Militzer, Phys. Rev. Lett. **108**, 115502 (2012).

[41] P. Giannozzi *et al.*, J. Phys. Condens. Matter **21**, 395 502 (2009).

[42] J. P. Perdew, K. Burke, and M. Ernzerhof, Phys. Rev. Lett. **77**, 3865 (1996). With enough empty-band states, the adoption of the cutoffs of 200 Ry for wave functions and 2000 Ry for the charge density ensures the convergence of the pressures and energies. (Enough band energies corresponding to unoccupied bands are considered to make the energies higher than $10k_BT$, promising the convergence of energy and pressure for every case.)

[43] See Supplemental Material at http://link.aps.org/supplemental/10.1103/PhysRevLett.109.175701 for calculation details, the EOS data, the definition of ECN, the persisted time length for the clusters, and details about the structure and charge density.

[44] A. Ghosh and H. J. Maris, Phys. Rev. Lett. **95**, 265 301 (2005).

[45] J. Faure, Y. Glinec, A. Pukhov, S. Kiselev, S. Gordienko, E. Lefebvre, J.-P. Rousseau, F. Burgy, and V. Malka, Nature (London) **431**, 541 (2004).

[46] D. Kang, J. Dai, and J. Yuan, J. Chem. Phys. **135**, 024 505 (2011).

[47] T. Ikeda, Y. Katayama, H. Saitoh, and K. Aoki, J. Chem. Phys. **132**, 121 102 (2010).

[48] E. Schwegler, G. Galli, F. Gygi, and R. Q. Hood, Phys. Rev. Lett. **87**, 265 501 (2001).

[49] J. Dai, Y. Hou, and J. Yuan, High Energy Density Phys. **7**, 84 (2011).

[50] M. J. Piotrowski, P. Piquini, and J. L. F. DaSilva, Phys. Rev. B **81**, 155446 (2010).

[51] Ya. Zeldovich and Yu. Raizer, *Physics of Shock Waves and High-Temperature Hydrodynamic Phenomena* (Academic, New York, 1966).

[52] Q. Porchero, G. Faussurier, and C. Blancard, High Energy Density Phys. **6**, 76 (2010); R. M. More, K. H. Warren, D. A. Young, and G. B. Zimmerman, Phys. Fluids **31**, 3059 (1988).

[53] G. M. Dyer *et al.*, Phys. Rev. Lett. **101**, 015002 (2008).

[54] A. K. Soper and C. J. Benmore, Phys. Rev. Lett. **101**, 065502 (2008); U. Bergmann, D. Nordlund, Ph. Wernet, M. Odelius, L. G. M. Pettersson, and A. Nilsson, Phys. Rev. B **76**, 024202 (2007).